

Scalable Asymptotically-Optimal Multi-Robot Motion Planning

Andrew Dobson

Kiril Solovey

Rahul Shome

Dan Halperin

Kostas E. Bekris

Abstract—Discovering high-quality paths for multi-robot problems can be achieved, in principle, through asymptotically-optimal data structures in the composite space of all robots, such as a sampling-based roadmap or a tree. The hardness of motion planning, however, which depends exponentially on the number of robots, renders the explicit construction of such structures impractical. This work proposes a scalable, sampling-based planner for coupled multi-robot problems that provides desirable path-quality guarantees. The proposed $dRRT^*$ is an informed, asymptotically-optimal extension of a prior method $dRRT$, which introduced the idea of building roadmaps for each robot and implicitly searching the tensor product of these structures in the composite space. The paper describes the conditions for convergence to optimal paths in multi-robot problems. Moreover, simulated experiments indicate $dRRT^*$ converges to high-quality paths and scales to higher numbers of robots where various alternatives fail. It can also be used on high-dimensional challenges, such as planning for robot manipulators.

I. INTRODUCTION AND PRIOR WORK

Many multi-robot planning applications [22], [4], [3] require high-dimensional platforms to simultaneously move in a shared workspace, where high-quality paths must be computed quickly as sensing input is updated, as in Fig. 1. Preprocessing given knowledge of the static scene can help the online computation of high-quality paths. Sampling-based roadmaps can help with such high-dimensional challenges and provide primitives for preprocessing a static scene [8], [9]. These methods converge to optimal solutions given sufficient density [7], i.e., at least $O(n \log(n))$ edges are needed for a roadmap with n vertices, while near-optimal solutions are achieved after finite computation time [2], [6].

Naïvely constructing a sampling-based roadmap or tree in the robots' composite configuration space provides asymptotic optimality but does not scale well. In particular, memory requirements depend exponentially

A. Dobson, R. Shome and K. E. Bekris are with the Computer Science Dept. of Rutgers University, NJ, USA, {chuples.dobson, rahul.shome, kostas.bekris}@cs.rutgers.edu. Their work is supported by NSF IIS 1451737 and NSF CCF 1330789.

K. Solovey and D. Halperin are with the Computer Science Dept. of Tel Aviv University, Israel, {kirilsol, danha}@post.tau.ac.il. Their work has been supported in part by the Israel Science Foundation (grant no. 825/15) and by the Blavatnik Computer Science Research Fund. K. S. has also been supported by the Clore Israel Foundation.

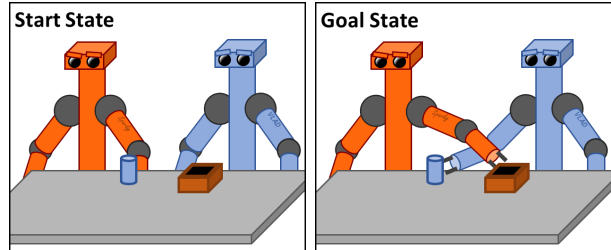


Fig. 1. Simultaneous planning for multiple high-dimensional systems is a difficult, motivating challenge for this work.

on the problem's dimension [15]. The alternative is decoupled planning, where paths for robots are computed independently and then coordinated [10]. These methods, however, typically lack completeness and optimality guarantees. Hybrid approaches can achieve optimal decoupling to retain guarantees [21]. The problem is more complex when the robots exhibit non-trivial dynamics [12]. Collision avoidance or control methods can scale to large numbers of robots, but typically lack global path quality guarantees [20], [19].

The previously proposed $dRRT$ approach [16] is a scalable sampling-based approach, which is probabilistically complete. It searches an implicit tensor product roadmap of roadmaps constructed for each robot individually [18]. The current work proposes $dRRT^*$ and shows that it is an efficient asymptotically optimal variant of the prior method. Simulations show the method practically generates high-quality paths while scaling to complex, high-dimensional problems, where alternatives fail.¹

II. PROBLEM SETUP AND NOTATION

Consider a shared workspace with $R \geq 2$ robots, each operating in configuration space \mathbb{C}_i for $1 \leq i \leq R$. Let $\mathbb{C}_i^f \subset \mathbb{C}_i$ be each robot's free space, where it is free from collision with the static scene, and $\mathbb{C}_i^o = \mathbb{C}_i \setminus \mathbb{C}_i^f$ is the forbidden space for robot i . The composite \mathbb{C} -space $\mathbb{C} = \prod_{i=1}^R \mathbb{C}_i$ is the Cartesian product of each robot's \mathbb{C} -space. A composite configuration $Q = (q_1, \dots, q_R) \in \mathbb{C}$ is an R -tuple of robot configurations. For two distinct robots i, j , denote by $I_i^j(q_j) \subset \mathbb{C}_i$ the set of configurations where i and j collide. Then, the

¹Additional material is provided in the appendices of this paper as well as the accompanying video of the original MRS submission.

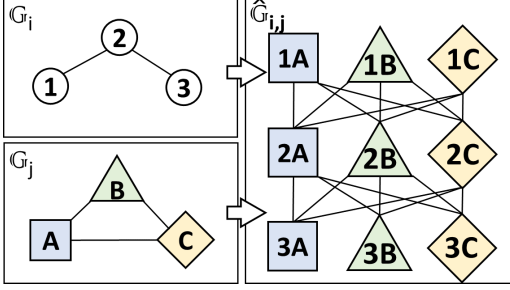


Fig. 2. An illustration of a two-robot tensor product roadmap $\hat{\mathbb{G}}_{i,j}$ between roadmaps \mathbb{G}_i and \mathbb{G}_j . Two nodes in the tensor-product roadmap share an edge if all the individual robot configurations share an edge in the individual robot roadmaps.

composite free space $\mathbb{C}^f \subset \mathbb{C}$ consists of configurations $Q = (q_1, \dots, q_R)$ subject to:

- $q_i \in \mathbb{C}_i^f$ for every $1 \leq i \leq R$;
- $q_i \notin I_i^j(q_j), q_j \notin I_j^i(q_i)$ for every $1 \leq i < j \leq R$.

Each $Q \in \mathbb{C}^f$ requires robots to not collide with obstacles, and each pair to not collide with each other. The composite forbidden space is defined as $\mathbb{C}^o = \mathbb{C} \setminus \mathbb{C}^f$.

Given $S, T \in \mathbb{C}^f$, where $S = (s_1, \dots, s_R), T = (t_1, \dots, t_R)$, a *trajectory* $\Sigma : [0, 1] \rightarrow \mathbb{C}^f$ is a continuous curve in \mathbb{C}^f , such that $\Sigma(0) = S, \Sigma(1) = T$, where the R robots move simultaneously. Σ is an R -tuple $(\sigma_1, \dots, \sigma_R)$ of robot paths such that $\sigma_i : [0, 1] \rightarrow \mathbb{C}_i^f$.

The objective is to find a trajectory which minimizes a *cost function* $c(\cdot)$. The analysis assumes the cost is the sum of robot path lengths, i.e., $c(\Sigma) = \sum_{i=1}^R |\sigma_i|$, where $|\sigma_i|$ denotes the standard *arc length* of σ_i . The arguments also work for $\max_{i=1:R} |\sigma_i|$.² Section IV shows sufficient conditions for dRRT* to converge to optimal trajectories over the cost function c .

III. METHODS FOR COMPOSITE SPACE PLANNING

For a fixed $n \in \mathbb{N}_+$, define for every robot i the PRM roadmap $\mathbb{G}_i = (\mathbb{V}_i, \mathbb{E}_i)$ constructed over \mathbb{C}_i^f , such that $|\mathbb{V}_i| = n$ with connection radius $r(n)$. Then, $\hat{\mathbb{G}} = (\hat{\mathbb{V}}, \hat{\mathbb{E}}) = \mathbb{G}_1 \times \dots \times \mathbb{G}_R$ is the *tensor product roadmap* in space \mathbb{C} (for an illustration, see Figure 2). Formally, $\hat{\mathbb{V}} = \{(v_1, v_2, \dots, v_R), \forall i, v_i \in \mathbb{V}_i\}$ is the Cartesian product of the nodes from each roadmap \mathbb{G}_i . For two vertices $V = (v_1, \dots, v_m) \in \hat{\mathbb{V}}, V' = (v'_1, \dots, v'_m) \in \hat{\mathbb{V}}$ the edge set $\hat{\mathbb{E}}$ contains edge (V, V') if for every i it is that $v_i = v'_i$ or $(v_i, v'_i) \in \mathbb{E}_i$.³

As shown in Algorithm 1, dRRT* grows a tree \mathbb{T} over $\hat{\mathbb{G}}$, rooted at the start configuration S and initializes path π_{best} (line 1). The method stores the node added each iteration V (Line 2), as part of an informed process to

guide the expansion of \mathbb{T} towards the goal. The method iteratively expands \mathbb{T} given a time budget (Line 3), as detailed by Algorithm 2, storing the newly added node V (Line 4). After expansion, the method traces the path which connects the source S with the target T (Line 5). If such a path is found, it is stored in π_{best} if it improves upon the cost of the previous solution (Lines 6, 7). Finally, the best path found π_{best} is returned (Line 8).

Algorithm 1: dRRT*($\hat{\mathbb{G}}, S, T$)

```

1  $\pi_{\text{best}} \leftarrow \emptyset, \mathbb{T}.\text{init}(S)$ ;
2  $V \leftarrow S$ ;
3 while  $\text{time.elapsed}() < \text{time\_limit}$  do
4    $V \leftarrow \text{Expand\_dRRT}^*(\hat{\mathbb{G}}, \mathbb{T}, V, T)$ ;
5    $\pi \leftarrow \text{Trace\_Path}(\mathbb{T}, S, T)$ ;
6   if  $\pi \neq \emptyset$  and  $\text{cost}(\pi) < \text{cost}(\pi_{\text{best}})$  then
7      $\pi_{\text{best}} \leftarrow \pi$ ;
8 return  $\pi_{\text{best}}$ 

```

The expansion step is given in Alg. 2. The default initial step of the method is given in Lines 1-4, i.e., when no V^{last} is passed (Line 1), which corresponds to an exploration step similar to RRT: a random sample Q^{rand} is generated in \mathbb{C} (Line 2), its nearest neighbor V^{near} in \mathbb{T} is found (Line 3) and the oracle function $\mathbb{O}_d(\cdot, \cdot)$ returns the implicit graph node V^{new} that is a neighbor of V^{near} on the implicit graph in the direction of Q^{rand} (Line 4). If a V^{last} , however, is provided (Line 5)—which happens when the last iteration managed to generate a node closer to the goal relative to its parent—then the V^{new} is greedily generated so as to be a neighbor of V^{last} in the direction of the goal T (Line 6).

In either case, the method next finds neighbors N , which are adjacent to V^{new} in $\hat{\mathbb{G}}$ and have also been added to \mathbb{T} (Line 7). Among N , the best node V^{best} is chosen, for which the local path $\mathbb{L}(V^{\text{best}}, V^{\text{new}})$ is collision-free and that the total path cost to V^{new} is minimized (Line 8). If no such parent can be found (Line 9), the expansion fails and no node is returned (Line 10). Then, if V^{new} is not in \mathbb{T} , it is added (Lines 11-13). Otherwise, if it exists, the tree is rewired so as to contain edge $(V^{\text{best}}, V^{\text{new}})$, and the cost of the V^{new} 's sub-tree (if any) is updated (Lines 14, 15). Then, for all nodes in N (Line 16), the method tests \mathbb{T} should be rewired through V^{new} to reach this neighbor. Given that $\mathbb{L}(V^{\text{new}}, v)$ is collision-free and is of lower cost than the existing path to v (Line 17), the tree is rewired to make V^{new} be the parent of v (line 18).

Finally, if in this iteration the heuristic value of V^{new} is lower than its parent node V^{best} (line 19), the method returns V^{new} (Line 20), causing the next iteration to greedily expand V^{new} . Otherwise, $NULL$ is returned

²The types of distances the arguments hold are more general, but proofs for alternative metrics are left as future work.

³Notice this slight difference from dRRT [16] so as to allow edges where some robots remain motionless while others move.

Algorithm 2: Expand_dRRT* ($\hat{\mathbb{G}}, \mathbb{T}, V^{\text{last}}, T$)

```

1 if  $V^{\text{last}} == \text{NULL}$  then
2   |  $Q^{\text{rand}} \leftarrow \text{Random\_Sample}();$ 
3   |  $V^{\text{near}} \leftarrow \text{Nearest\_Neighbor}(\mathbb{T}, Q^{\text{rand}});$ 
4   |  $V^{\text{new}} \leftarrow \mathbb{O}_d(V^{\text{near}}, Q^{\text{rand}});$ 
5 else
6   |  $V^{\text{new}} \leftarrow \mathbb{O}_d(V^{\text{last}}, T);$ 
7   |  $N \leftarrow \text{Adjacent}(V^{\text{new}}, \hat{\mathbb{G}}) \cap \mathbb{V}_T;$ 
8   |  $V^{\text{best}} \leftarrow$ 
      |  $\arg \min_{v \in N, s.t. \mathbb{L}(v, V^{\text{new}}) \subset \mathbb{C}^f} c(v) + c(\mathbb{L}(v, V^{\text{new}}));$ 
9   | if  $V^{\text{best}} == \text{NULL}$  then
10    | return  $\text{NULL};$ 
11   | if  $V^{\text{new}} \notin \mathbb{T}$  then
12    |  $\mathbb{T}.\text{Add\_Vertex}(V^{\text{new}});$ 
13    |  $\mathbb{T}.\text{Add\_Edge}(V^{\text{best}}, V^{\text{new}});$ 
14   | else
15    |  $\mathbb{T}.\text{Rewire}(V^{\text{best}}, V^{\text{new}});$ 
16   | for  $v \in N$  do
17    | if  $c(V^{\text{new}}) + c(\mathbb{L}(V^{\text{new}}, v)) < c(v)$  and
      |  $\mathbb{L}(V^{\text{new}}, v) \subset \mathbb{C}^f$  then
18    | |  $\mathbb{T}.\text{Rewire}(V^{\text{new}}, v);$ 
19   | if  $h(V^{\text{new}}) < h(V^{\text{best}})$  then
20    | return  $V^{\text{new}};$ 
21   | else
22    | return  $\text{NULL};$ 

```

so as to do an exploration step. Note that the approach is implemented with helpful branch-and-bound pruning after an initial solution is found, though this is not reflected in the algorithmics.

V^{new} is determined via an oracle function. Using this oracle function and a simple rewiring scheme is sufficient for showing asymptotic optimality for dRRT* (see Section IV). The oracle function \mathbb{O}_d for a two-robot case is illustrated in Figure 3. First, let $\rho(Q, Q')$ be the ray from configuration Q terminating at Q' . Then, denote $\angle_Q(Q', Q'')$ as the minimum angle between $\rho(Q, Q')$ and $\rho(Q, Q'')$. When Q^{rand} is drawn in \mathbb{C} , its nearest neighbor V^{near} in \mathbb{T} is found. Then, project the points Q^{rand} and V^{near} into each robot space \mathbb{C}_i , i.e., ignore the configurations of other robots.

The method separately searches the single-robot roadmaps to discover V^{new} . Denote $V^{\text{near}} = (v_1, \dots, v_R), Q^{\text{rand}} = (\tilde{q}_1, \dots, \tilde{q}_R)$. For every robot i , let $N_i \subset \mathbb{V}_i$ be the neighborhood of $v_i \in \mathbb{V}_i$, and identify $v'_i = \arg \min_{v \in N_i} \angle_{v_i}(q_i^{\text{rand}}, v)$. The oracle function returns node $V^{\text{new}} = (v'_1, \dots, v'_R)$.

As in the standard RRT as well as in dRRT, the dRRT* approach has a Voronoi-bias property [11]. It is, however, slightly more involved to observe as shown in Figure 4. To generate an edge (V, V') , random sample

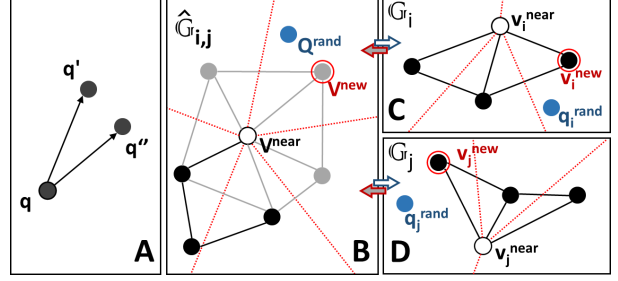


Fig. 3. (A) The method reasons over all neighbors q' of q so as to minimize the angle $\angle_q(q', q'')$. (B) $\mathbb{O}_d(\cdot, \cdot)$ finds graph vertex V^{new} by minimizing angle $\angle_{V^{\text{near}}}(V^{\text{new}}, Q^{\text{rand}})$. (C,D) V^{near} and Q^{rand} are projected into each robot's \mathbb{C} -space so as to find nodes v_i^{new} and v_j^{new} , respectively, which minimize angle $\angle_{v_i^{\text{near}}}(v_i^{\text{new}}, q_i^{\text{rand}})$.

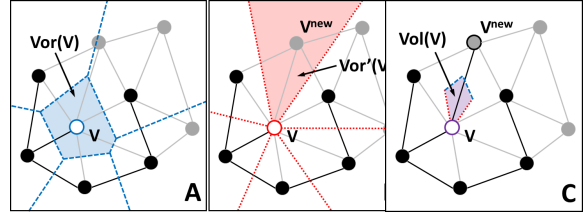


Fig. 4. (A) The Voronoi region $\text{Vor}(V)$ of vertex V is shown where if Q^{rand} is drawn, vertex V is selected for expansion. (B) When Q^{rand} lies in the directional Voronoi region $\text{Vor}'(V)$, the expand step expands to V^{new} . (C) Thus, when Q^{rand} is drawn within volume $\text{Vol}(V) = \text{Vor}(V) \cup \text{Vor}'(V)$, the method will generate V^{new} via V .

Q^{rand} must be drawn within the Voronoi cell of V , denoted $\text{Vor}(V)$ (A) and in the general direction of V' , denoted $\text{Vor}'(V)$ (B). The intersection of these two volumes $\text{Vol}(V) = \text{Vor}(V) \cap \text{Vor}'(V)$ is the volume to be sampled generate V^{new} via V^{near} .

IV. ANALYSIS

In this section, the theoretical properties of dRRT* are examined, beginning with a study of the asymptotic convergence of the implicit roadmap $\hat{\mathbb{G}}$ to containing a path in \mathbb{C}^f whose cost converges to the optimum. Then, it is shown dRRT* eventually discovers the shortest path in $\hat{\mathbb{G}}$, and that the combination of these two facts proves the asymptotic optimality of dRRT*.

For simplicity, the analysis is restricted to the setting of robots operating in Euclidean space, i.e. \mathbb{C}_i is a d -dimensional Euclidean hypercube $[0, 1]^d$ for fixed $d \geq 2$.⁴ Additionally, the analysis is restricted to the specific cost function of *total distance*, i.e., $|\Sigma| := \sum_{i=1}^R |\sigma_i|$. Discussion on lifting these restrictions is provided in Section VI.

A. Optimal Convergence of $\hat{\mathbb{G}}$

For each robot, an asymptotically optimal PRM* roadmap \mathbb{G}_i is constructed having n samples and using

⁴For simplicity, it is assumed that all the robots have the same number of degrees of freedom d .

a connection radius $r(n)$ necessary for asymptotic convergence to the optimum [7]. By the nature of sampling-based algorithms, each graph cannot converge to the true optimum with finite computation, as such a solution may have clearance of exactly 0. Instead, this work focuses on the notion of a robust optimum⁵, showing that the tensor product roadmap $\hat{\mathbb{G}}$ converges to this value.

Definition 1: A trajectory $\Sigma : [0, 1] \rightarrow \mathbb{C}^f$ is *robust* if there exists a fixed $\delta > 0$ such that for every $\tau \in [0, 1], X \in \mathbb{C}^o$ it holds that $\|\Sigma(\tau) - X\|_2 \geq \delta$, where $\|\cdot\|_2$ denotes the standard Euclidean distance.

Definition 2: A value $c > 0$ which denotes a path cost is robust if for every fixed $\epsilon > 0$ there exists a robust path Σ such that $|\Sigma| \leq (1 + \epsilon)c$. The *robust optimum*, denoted by c^* , is the infimum over all such values.

For any fixed $n \in \mathbb{N}^+$, and a specific instance of $\hat{\mathbb{G}}$ constructed from R roadmaps, having n samples each, denote by $\Sigma^{(n)}$ the shortest path from S to T over $\hat{\mathbb{G}}$.

Definition 3: $\hat{\mathbb{G}}$ is asymptotically optimal (AO) if for every fixed $\epsilon > 0$ it holds that $|\Sigma^{(n)}| \leq (1 + \epsilon)c^*$ a.a.s.⁶, where the probability is over all the instantiations of $\hat{\mathbb{G}}$ with n samples for each PRM.

Using this definition, the following theorem is proven. Recall that d denotes the dimension of a single-robot configuration space.

Theorem 1: $\hat{\mathbb{G}}$ is AO when

$$r(n) \geq r^*(n) = (1 + \eta)2 \left(\frac{1}{d}\right)^{\frac{1}{d}} \left(\frac{\log n}{n}\right)^{\frac{1}{d}},$$

where η is any constant larger than 0.

Remark. Note that $r^*(n)$ was developed in [6, Theorem 4.1], and guarantees AO of PRM* for a single robot. The proof technique described in that work will be one of the ingredients used to prove Theorem 1.⁷

By definition of c^* , for any given $\epsilon > 0$ there exists robust trajectory $\Sigma : [0, 1] \rightarrow \mathbb{C}^f$, and fixed $\delta > 0$, such that the cost of Σ is at most $(1 + 1/2 \cdot \epsilon)c^*$ and for every $X \in \mathbb{C}^o, \tau \in [0, 1]$ it holds that $\|\Sigma(\tau) - X\| \geq \delta$. Next, it is shown that $\hat{\mathbb{G}}$ contains a trajectory $\Sigma^{(n)}$ such that

$$|\Sigma^{(n)}| \leq (1 + o(1)) \cdot |\Sigma|, \quad (1)$$

a.a.s.. This immediately implies that $|\Sigma^{(n)}| \leq (1 + \epsilon)c^*$, which will finish the proof of Theorem 1.

Thus, it remains to show that there exists a trajectory on $\hat{\mathbb{G}}$ which satisfies Equation 1 a.a.s.. As a first step, it will be shown that the robustness of $\Sigma = (\sigma_1, \dots, \sigma_R)$

⁵Note that the given definition of robust optimum is similar to that in previous work [17].

⁶Let A_1, A_2, \dots be random variables in some probability space and let B be an event depending on A_n . We say that B occurs *asymptotically almost surely* (a.a.s.) if $\lim_{n \rightarrow \infty} \Pr[B(A_n)] = 1$.

⁷Note that $r^*(n)$ can be refined to incorporate the proportion of \mathbb{C}_i^f , which would reduce this expression.

in the composite space implies robustness in the single-robot setting, i.e., robustness along σ_i .

For $\tau \in [0, 1]$ define the forbidden space parameterized by τ as

$$\mathbb{C}_i^o(\tau) = \mathbb{C}_i^o \cup \bigcup_{j=1, j \neq i}^R I_i^j(\sigma_j(\tau)).$$

Claim 1: For every robot $i, \tau \in [0, 1]$, and $q_i \in \mathbb{C}_i^o(\tau), \|\sigma_i(\tau) - q_i\|_2 \geq \delta$.

Proof: Fix a robot i , and fix some $\tau \in [0, 1]$ and a configuration $q_i \in \mathbb{C}_i^o(\tau)$. Next, define the following composite configuration

$$Q = (\sigma^1(\tau), \dots, q_i, \dots, \sigma^R(\tau)).$$

Note that it differs from $\Sigma(\tau)$ only in the i -th robot's configuration. By the robustness of Σ it follows that

$$\begin{aligned} \delta &\leq \|\Sigma(\tau) - Q\|_2 \\ &= \left(\|\sigma_i(\tau) - q_i\|_2^2 + \sum_{j=1, j \neq i}^R \|\sigma_j(\tau) - \sigma_j(\tau)\|_2^2 \right)^{\frac{1}{2}} \\ &\leq \|\sigma_i(\tau) - q_i\|_2. \end{aligned}$$

The result of claim 1 is that the paths $\sigma_1, \dots, \sigma_R$ are robust in the sense that there is sufficient clearance for the individual robots to not collide with each other given a fixed location of a single robot. A Lemma is derived using proof techniques from the literature [6], and it implies every \mathbb{G}_i contains a single-robot path $\sigma_i^{(n)}$ that converges to σ_i .

Lemma 1: For every robot i, \mathbb{G}_i constructed with n samples and a connection radius $r(n) \geq r^*(n)$ contains a path $\sigma_i^{(n)}$ with the following attributes a.a.s.:

- (i) $\sigma_i^{(n)}(0) = s_i, \sigma_i^{(n)}(1) = t_i$;
- (ii) $|\sigma_i^{(n)}| \leq (1 + o(1))|\sigma_i|$;
- (iii) $\forall q \in \text{Im}(\sigma_i^{(n)}), \exists \tau \in [0, 1]$ s.t. $\|q - \sigma_i(\tau)\|_2 \leq r^*(n)$.

Proof: The first property (i) follows from the fact that s_i, t_i are directly added to \mathbb{G}_i . The rest follows from the proof of Theorem 4.1 in [6], which is applicable here since $r(n) \geq r^*(n)$.

Lemma 1 also implies that $\hat{\mathbb{G}}$ contains a path in \mathbb{C} , that represents robot-to-obstacle collision-free motions, and minimizes the multi-robot metric cost. In particular, define $\Sigma^{(n)} = (\sigma_1^{(n)}, \dots, \sigma_R^{(n)})$, where $\sigma_i^{(n)}$ are obtained from Lemma 1. Then

$$|\Sigma^{(n)}| = \sum_{i=1}^R |\sigma_i^{(n)}| \leq (1 + o(1)) \sum_{i=1}^R |\sigma_i| \leq (1 + o(1))|\Sigma|.$$

However, it is not clear whether this ensures the existence of a path where robot-robot collisions are avoided. That is, although $\text{Im}(\sigma_i^{(n)}) \subset \mathbb{C}_i^f$, it might be the case that $\text{Im}(\Sigma^{(n)}) \cap \mathbb{C}^o \neq \emptyset$. Next it is shown that $\sigma_1^{(n)}, \dots, \sigma_R^{(n)}$ can be reparametrized to induce a

composite-space path whose image is fully contained in \mathbb{C}^f , with length equivalent to $\Sigma^{(n)}$.

For each robot i , denote by $V_i = (v_i^1, \dots, v_i^{\ell_i})$ the chain of \mathbb{G}_i vertices traversed by $\sigma_i^{(n)}$. For every $v_i^j \in V_i$ assign a timestamp τ_i^j of the closest configuration along σ_i , i.e.,

$$\tau_i^j = \arg \min_{\tau \in [0,1]} \|v_i^j - \sigma_i(\tau)\|_2.$$

Also, define $\mathcal{T}_i = (\tau_i^1, \dots, \tau_i^{\ell_i})$ and denote by \mathcal{T} the ordered list of $\bigcup_{i=1}^R \mathcal{T}_i$, according to the timestamp values. Now, for every i , define a global timestamp function $TS_i : \mathcal{T} \rightarrow V_i$ which assigns to each global timestamp in \mathcal{T} a single-robot configuration from V_i . It thus specifies in which vertex robot i resides at time $\tau \in \mathcal{T}$. For $\tau \in \mathcal{T}$, let j be the largest index such that $\tau_i^j \leq \tau$. Then simply assign $TS_i(\tau) = v_i^j$. From property (iii) in Lemma 1 and Claim 1 it follows that no robot-robot collisions are induced by the reparametrization, concluding the proof of Theorem 1.

B. Asymptotic Optimality of dRRRT*

Finally, dRRRT* is shown to be AO. Denote by m the time budget in Algorithm 1, i.e., the number of iterations of the loop. Denote by $\Sigma^{(n,m)}$ the solution returned by dRRRT* for n and m .

Theorem 2: If $r(n) > r^*(n)$ then for every fixed $\epsilon > 0$ it holds that

$$\lim_{n,m \rightarrow \infty} \Pr \left[|\Sigma^{(n,m)}| \leq (1 + \epsilon)c^* \right] = 1.$$

Since $\hat{\mathbb{G}}$ is AO (Theorem 1), it suffices to show that for any fixed n , and a fixed instance of $\hat{\mathbb{G}}$, defined over R PRMs with n samples each, dRRRT* eventually (as m tends to infinity), finds the optimal trajectory over $\hat{\mathbb{G}}$. This can be shown using the properties of a Markov chain with absorbing states [5, Theorem 11.3]. While a full proof is omitted here, the high-level idea is similar to what is presented in previous work [16, Theorem 3], and expanded upon in Appendix A. By restricting the states of the Markov chain to being the graph vertices along the optimal path, setting the target vertex to be an absorbing vertex, and showing that the probability of transitioning along any edge in this path is nonzero (i.e. the probability is proportional to $\frac{\mu(\text{Vol}(V_k))}{\mu(\mathbb{C}^f)} > 0$), then the probability that this process does not reach the target state along the optimal path converges to 0 as the number of dRRRT* iterations tends to infinity. The final step is to show that the above statements hold when both m and n tend to ∞ . A proof for this phenomenon can be found in [16, Theorem 6].

V. EXPERIMENTAL VALIDATION

This section provides an experimental evaluation of dRRRT* by demonstrating practical convergence, scala-

bility, and applicability to dual-arm manipulation. The approach and alternatives are executed on a cluster with Intel(R) Xeon(R) CPU E5-4650 @ 2.70GHz processors, and 128GB of RAM. ⁸

2 Disk Robots among 2D Polygons:

This base-case test involves 2 disks ($\mathbb{C}_i := \mathbb{R}^2$) of radius 0.2, in a 10.2×10.2 region, as in Figure 5. The disks have to swap positions between $(0,0)$ and $(9,9)$. This is a setup where it is possible to compute the explicit

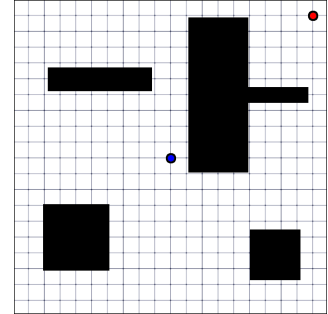


Fig. 5. The 2D environment where the 2 disk robots operate.

roadmap, which is not practical in more involved scenarios. In particular, dRRRT* is tested against: a) running A* on the implicit tensor roadmap $\hat{\mathbb{G}}$ (referred to as “Implicit A*”) defined over the same individual roadmaps with N nodes each as those used by dRRRT*; and b) an explicitly constructed PRM* roadmap with N^2 nodes in the composite space.

Results are shown in Figure 6. dRRRT* converges to the optimal path over $\hat{\mathbb{G}}$, similar to the one discovered by Implicit A*, while quickly finding an initial solution of high quality. Furthermore, the implicit tensor product roadmap $\hat{\mathbb{G}}$ is of comparable quality to the explicitly constructed roadmap.

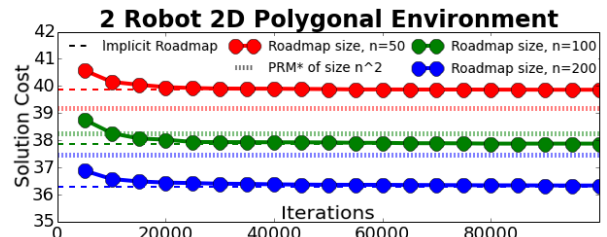


Fig. 6. Average solution cost over iterations. Data averaged over 10 roadmap pairs. dRRRT* (solid line) converges to the optimal path through $\hat{\mathbb{G}}$ (dashed line).

Table I presents running times. dRRRT* and implicit A* construct 2 N -sized roadmaps (row 3), which are faster to construct than the PRM* roadmap in \mathbb{C} (row 1). PRM* becomes very costly as N increases. For $N = 500$, the explicit roadmap contains 250,000 vertices, taking 1.7GB of RAM to store, which was the upper limit for the machine used. When the roadmap can be constructed, it is quicker to query (row 2). dRRRT* quickly returns an initial solution (row 5), and converges within 5% of the optimum length (row 6) well before Implicit

⁸Additional data are provided in Appendix B.

A^* returns a solution as N increases (row 4). The next benchmark further emphasizes this point.

TABLE I

CONSTRUCTION AND QUERY TIMES (SECS) FOR 2 DISK ROBOTS.

Number of nodes: $N =$	50	100	200
N^2 -PRM* construction	3.427	13.293	69.551
N^2 -PRM* query	0.002	0.004	0.023
2 N -size PRM* construction	0.1351	0.274	0.558
Implicit A^* search over \mathbb{G}	0.684	2.497	10.184
dRRT* over \mathbb{G} (initial)	0.343	0.257	0.358
dRRT* over \mathbb{G} (converged)	3.497	4.418	5.429

Many Disk Robots among 2D Polygons: In the same environment as above, the number of robots R is increased to evaluate scalability. Each robot starts on the perimeter of the environment and is tasked with reaching the opposite side. An $N = 50$ roadmap is constructed for every robot. It quickly becomes intractable to construct a PRM* roadmap in the composite space of many robots.

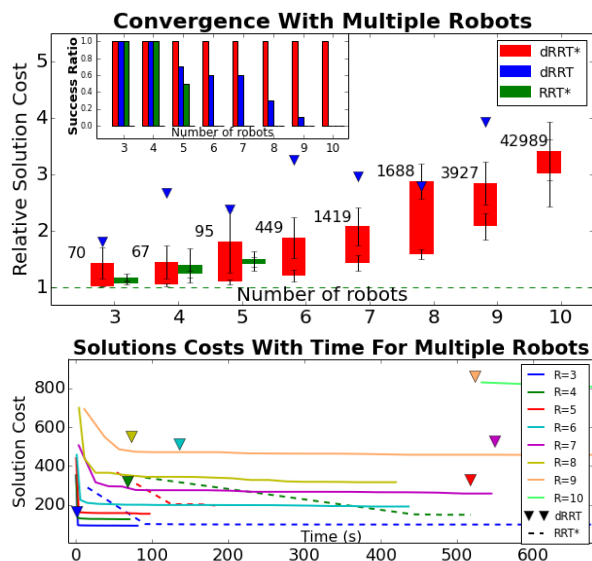


Fig. 7. Data averaged over 10 runs. (Top): Relative solution cost and success ratio of dRRT*, dRRT and RRT* for increasing R . dRRT*: average iteration and variance for initial solution (top of box), and solution cost and variance after 100,000 iterations (bottom). Similar results for RRT*. Single data point for dRRT (no quality improvement after first solution). (Bottom): Solution costs over time.

Figure 7 shows the inability of alternatives to compete with dRRT* in scalability. Solution costs are normalized by an optimistic estimate of the path cost for each case, which is the sum of the optimal solutions for each robot, disregarding robot-robot interactions. Implicit A^* fails to return solutions even for 3 robots. Directly executing RRT* in the composite space fails to do so for $R \geq 6$. The original dRRT method (without the informed search component) starts suffering in success ratio for $R \geq 5$ and returns worse solutions than dRRT*. The average solution times for dRRT may decrease as R increases

but this is due to the decreasing success ratio, i.e., dRRT begins to only succeed at easy problems.

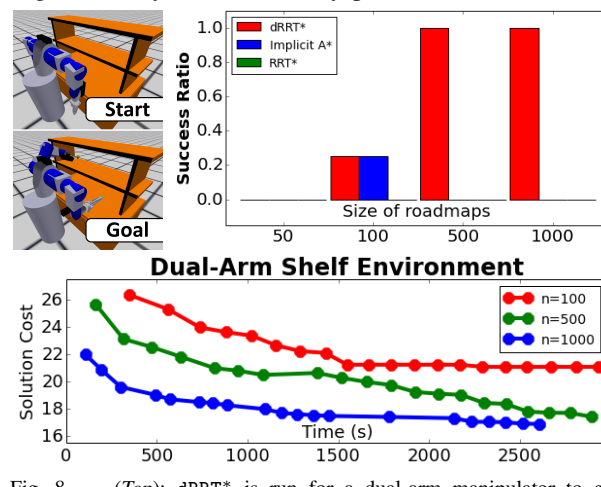


Fig. 8. (Top): dRRT* is run for a dual-arm manipulator to go from its home position (above) to a reaching configuration (below) and achieves perfect success ratio as n increases. (Bottom): dRRT* solution quality over time. Here, larger roadmaps provide benefits in terms of running time and solution quality.

Dual-arm manipulator: This test shows the benefits of dRRT* when planing for two 7-dimensional arms. Figure 8 shows that RRT* fails to return solutions within 100K iterations. Using small roadmaps is also insufficient for this problem. Both dRRT* and Implicit A^* require larger roadmaps to begin succeeding. But with $N \geq 500$, Implicit A^* always fails, while dRRT* maintains a 100% success ratio. As expected, roadmaps of increasing size result in higher quality path. The informed nature of dRRT* also allows to find initial solutions fast, which together with the branch-and-bound primitive allows for good convergence.

VI. DISCUSSION

This work studies the asymptotic optimality of sampling-based multi-robot planning over implicit structures. The objective is to efficiently search the composite space of multi-robot systems while also achieving formal guarantees. This requires construction of asymptotically optimal individual robot roadmaps and appropriately searching their tensor product. Performance is further improved by informed search in the composite space.

These results may extend to more complex settings involving kinodynamic constraints by relying on recent work [14], [13]. Furthermore, the analysis may be valid for different cost functions other than total distance. The tools presented here can prove useful in the context of simultaneous task and motion planning for multiple robots, especially manipulators [1].

REFERENCES

- [1] A. Dobson and K. E. Bekris. Planning Representations and Algorithms for Prehensile Multi-Arm Manipulation. In *IEEE/RSJ International Conference on Intelligent Robots and Systems (IROS)*, 2015.
- [2] A. Dobson, G. Moustakides, and K. E. Bekris. Geometric Probability Results For Bounding Path Quality In Sampling-Based Roadmaps After Finite Computation. In *IEEE Inter. Conf. on Robotics and Automation (ICRA)*, 2015.
- [3] M. Gharbi, J. Cortés, and T. Siméon. Roadmap Composition for Multi-Arm Systems Path Planning. In *IEEE/RSJ International Conference on Intelligent Robots and Systems (IROS)*, 2009.
- [4] F. Gravit and R. Alami. A Method for Handling Multiple Roadmaps and Its Use for Complex Manipulation Planning. In *IEEE International Conference on Robotics and Automation (ICRA)*, 2003.
- [5] C. Grinstead and J. Snell. *Introduction to Probability*. American Mathematical Society, Providence, RI, 2012.
- [6] L. Janson, A. Schmerling, A. Clark, and M. Pavone. Fast Marching Tree: a Fast marching Sampling-Based Method for Optimal Motion Planning in Many Dimensions. *International Journal of Robotics Research (IJRR)*, 34(7):883–921, 2015.
- [7] S. Karaman and E. Frazzoli. Sampling-based Algorithms for Optimal Motion Planning. *International Journal of Robotics Research (IJRR)*, 30(7):846–894, June 2011.
- [8] L. E. Kavraki, P. Svestka, J.-C. Latombe, and M. Overmars. Probabilistic Roadmaps for Path Planning in High-Dimensional Configuration Spaces. *IEEE Transactions on Robotics and Automation*, 12(4):566–580, 1996.
- [9] S. M. LaValle and J. J. Kuffner. Randomized Kinodynamic Planning. *International Journal of Robotics Research (IJRR)*, 20:378–400, May 2001.
- [10] S. Leroy, J. Laumond, and Siméon. Multiple Path Coordination for Mobile Robots: A Geometric Algorithm. Barcelona, Catalonia, Spain, 1999. International Joint Conference on Artificial Intelligence (IJCAI).
- [11] S. R. Lindemann and S. M. LaValle. Incrementally reducing dispersion by increasing voronoi bias in rrts. In *Proceedings of the 2004 IEEE International Conference on Robotics and Automation, ICRA 2004, April 26 - May 1, 2004, New Orleans, LA, USA*, pages 3251–3257, 2004.
- [12] J. Peng and S. Akella. Coordinating Multiple Robots with Kinodynamic Constraints Along Specified Paths. *The International Journal of Robotics Research*, 24(4):295–310, 2005.
- [13] E. Schmerling, L. Janson, and M. Pavone. Optimal sampling-based motion planning under differential constraints: The drift case with linear affine dynamics. In *54th IEEE Conference on Decision and Control, CDC 2015, Osaka, Japan, December 15-18, 2015*, pages 2574–2581, 2015.
- [14] E. Schmerling, L. Janson, and M. Pavone. Optimal sampling-based motion planning under differential constraints: The driftless case. In *IEEE International Conference on Robotics and Automation, ICRA 2015, Seattle, WA, USA, 26-30 May, 2015*, pages 2368–2375, 2015.
- [15] J. T. Schwartz and M. Sharir. On the Piano Movers’ Problem: III. Coordinating the Motion of Several Independent Bodies: The Special Case of Circular Bodies Moving Amidst Polygonal Barriers. *The International Journal of Robotics Research*, 2(3):46–75, 1983.
- [16] K. Solovey, O. Salzman, and D. Halperin. Finding a needle in an exponential haystack: Discrete RRT for exploration of implicit roadmaps in multi-robot motion planning. *I. J. Robotics Res.*, 35(5):501–513, 2016.
- [17] K. Solovey, O. Salzman, and D. Halperin. New Perspective on Sampling-based Motion Planning via Random Geometric Graphs. In *Robotics Science and Systems (RSS)*, 2016.
- [18] P. Svestka and M. Overmars. Coordinated Path Planning for Multiple Robots. *Robotics and Autonomous Systems*, 23:125–152, 1998.
- [19] S. Tang and V. Kumar. A Complete Algorithm for Generating Safe Trajectories for Multi-Robot Teams. In *International Symposium on Robotics Research (ISRR)*, Sestri Levante, Italy, September 2015.
- [20] J. Van Den Berg, S. Guy, M. Lin, and D. Manocha. *Reciprocal n-body collision avoidance*, volume 70 of *Springer Tracts in Advanced Robotics*, pages 3–19. Star edition, 2011.
- [21] J. van den Berg, J. Snoeyink, M. Lin, and D. Manocha. Centralized Path Planning for Multiple Robots: Optimal Decoupling into Sequential Plans. In *Robotics: Science and Systems (RSS)*, 2009.
- [22] G. Wagner and H. Choset. Subdimensional Expansion for Multi-robot Path Planning. *Artificial Intelligence Journal*, 219:1024, 2015.

APPENDIX

A. Proof of Convergence

This appendix examines the result of Theorem 2, and formally proves the convergence of the dRRT* tree toward containing all optimal paths.

Lemma 2 (Optimal Tree Convergence of dRRT*):

Consider an arbitrary optimal path π^* originating from v_0 and ending at v_t , then let $O_k^{(m)}$ be the event such that after m iterations of dRRT*, the search tree \mathbb{T} contains the optimal path up to segment k . Then,

$$\liminf_{m \rightarrow \infty} \mathbb{P}(O_t^{(m)}) = 1.$$

Proof. This property will be proven using a theorem from Markov chain literature [5, Theorem 11.3]. Specifically, the properties of absorbing Markov chains can be exploited to show that dRRT* will eventually contain the optimal path over $\hat{\mathbb{G}}$ for a given query. An absorbing Markov chain is one such that there is some subset of states in which the transition matrix only allows that state to transition to itself.

The proof follows by showing that the dRRT* method can be described as an absorbing Markov chain, where the target state of a query is represented as an absorbing state in a Markov chain, re-stated here.

Theorem 3 (Thm 11.3 in Grinstead & Snell):

In an absorbing Markov chain, the probability that the process will be absorbed is 1 (i.e., $Q(m) \rightarrow 0$ as $n \rightarrow \infty$), where $Q(m)$ is the transition submatrix for all non-absorbing states.

There are two steps to using this proof. First, that the dRRT* search can be cast as an absorbing Markov chain, and second, that the probability of transition for from each state to the next in this chain is nonzero (i.e. that each state can eventually be connected to the target).

For query (S, T) , let the sequence $V = \{v_1, v_2, \dots, v_t\}$ of length t represent the vertices of $\hat{\mathbb{G}}$ corresponding to the optimal path through the graph which connects these points, where v_t

corresponds to the target vertex, and furthermore, let v_t be an absorbing state. Theorem 3 operates under the assumption that each vertex v_i is connected to an absorbing state (v_t in this case).

Then, let the transition probability for each state have two values, one for each state transitioning to itself, which corresponds to the dRRT* search expanding along some other arbitrary path. The other value is a transition probability from v_i to v_{i+1} . This corresponds to the method sampling within the volume $\text{Vol}(v_i)$.

Then, as the second step, it must be shown that this volume has a positive probability of being sampled in each iteration. It is sufficient then to argue that $\frac{\mu(\text{Vol}(s_i))}{\mu(C^i)} > 0$. Fortunately, for any finite n , previous work has already shown that this is the case given general position assumptions [16, Lemma 2].

Given these results, the dRRT* is cast as an absorbing Markov chain which satisfies the assumptions of 3, and therefore, the matrix $Q(m) \rightarrow 0$. This implies that the optimal path to the goal has been expanded in the tree, and therefore $\liminf_{m \rightarrow \infty} \mathbb{P}(O_t^{(m)}) = 1$. \square

B. More Experimental Data

This appendix presents additional experimental data omitted from Section V.

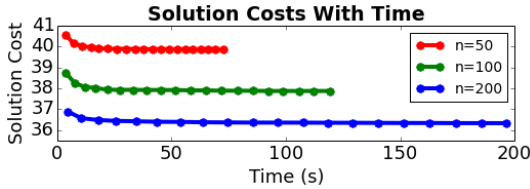


Fig. 9. 2-Robot convergence data over time.

1) *2-Robot Benchmark*: For the two-robot benchmark, additional data is presented in Figure 9. Here, the data presented in Figure 6 is shown again over time instead of over iterations.

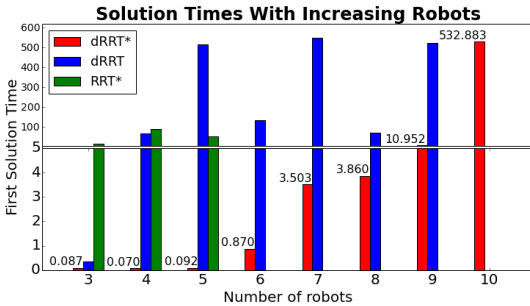


Fig. 10. R -robot solution times for varying R .

2) *R-Robot Benchmark*: For the R -robot benchmark, additional data is presented in Figure 10, showing query resolution times for the various methods.

To emphasize the lack of scalability for alternate methods, additional experiments were run in this setup

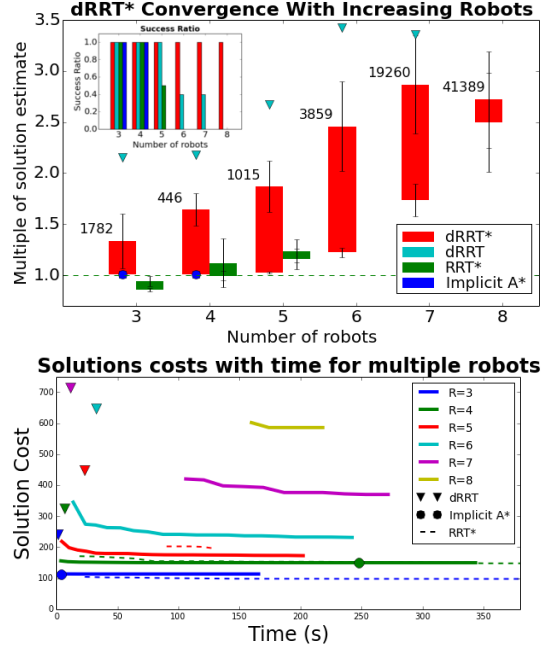


Fig. 11. (Top): Convergence rate and success ratio over the minimal 9-node roadmap (Bottom): Solution cost over time when using the minimal roadmap.

using a minimal roadmap. The tests use a 9-node roadmap for each robot as illustrated in Figure 12. Each roadmap is constructed with slight perturbations to the nodes within the shaded regions indicated in the figure.

The data for this modified benchmark (shown in Figure 11) indicate that even using a very small roadmap does not allow alternate methods to scale. While the methods scale better, Implicit A* does time out for $R \geq 5$, and RRT* times out for $R \geq 6$.

3) Manipulator Benchmark:

For the dual-arm manipulator benchmark, additional data is presented in Figure 13. Here, the data of Figure 8 is shown over iterations instead of over time.

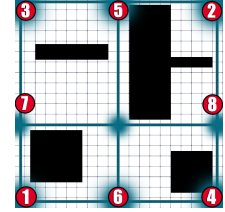


Fig. 12. Minimal graph for the R -robot case.

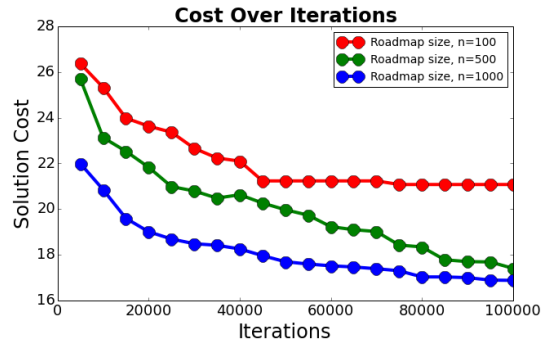


Fig. 13. Motoman benchmark solution quality over iterations.